High operating temperature midwave quantum dot barrier infrared detector (QD-BIRD)

David Z. Ting*, Alexander Soibel, Cory J. Hill, Sam A. Keo,
Jason M. Mumolo, and Sarath D. Gunapala

Center for Infrared Sensors
Jet Propulsion Laboratory
California Institute of Technology
4800 Oak Grove Drive, Pasadena, California, USA 91109-8099

ABSTRACT

The nBn or XBn barrier infrared detector has the advantage of reduced dark current resulting from suppressed Shockley-Read-Hall (SRH) recombination and surface leakage. High performance detectors and focal plane arrays (FPAs) based on InAsSb absorber lattice matched to GaSb substrate, with a matching AlAsSb unipolar electron barrier, have been demonstrated. The band gap of lattice-matched InAsSb yields a detector cutoff wavelength of approximately 4.2 • μm when operating at ~150K. We report results on extending the cutoff wavelength of midwave barrier infrared detectors by incorporating self-assembled InSb quantum dots into the active area of the detector. Using this approach, we were able to extend the detector cutoff wavelength to ~6 μm, allowing the coverage of the full midwave infrared (MWIR) transmission window. The quantum dot barrier infrared detector (QD-BIRD) shows infrared response at temperatures up to 225 K.

Keywords: midwave infrared, high operating temperature, infrared detector, quantum dot, unipolar barrier

1. INTRODUCTION

The recent emergence of barrier infrared detectors such as the nBn [1] and the XBn [2] have resulted in mid-wave infrared (MWIR) detectors with substantially higher operating temperatures than previously available in III-V semiconductor based MWIR detectors. The initial nBn devices used either InAs absorber grown on InAs substrate, or lattice-matched InAsSb alloy grown on GaSb substrate, with cutoff wavelengths of ~3.2 μm and ~4 μm, respectively. While these detectors could operate at much higher temperatures than existing MWIR detectors based on InSb, their spectral responses do not cover the full (3 – 5 μm) MWIR atmospheric transmission window. This has led to the development of nBn detectors such as those based on the InAs/GaSb type-II superlattice (T2SL) absorber [3,4] . In this paper, we describe our effort in combining the unipolar barrier infrared detector device architecture with alternative infrared absorbers based on InSb quantum dot embedded an InAsSb matrix in order to achieve extended spectral coverage [5]. We discuss the general unipolar barrier infrared detector device architecture in Section 2, the specific quantum dot barrier infrared detector (QD-BIRD) in Section 3, and summarize Sections 4.

* David.Z.Ting@jpl.nasa.gov; Ph: +1.818.354.1549; FAX: +1.818.393.4663

2. BARRIER INFRARED DETECTORS

In this section, we examine the concept of unipolar barriers and explore their use in infrared detectors. We discuss the specific example of the nBn infrared detector to illustrate the usefulness of unipolar barriers.

2.1 Unipolar barriers

The use of heterostructures to improve HgCdTe (MCT) infrared detector performance is a well-established practice [6,7,8]. Detector structures such as the double-layer heterojunction (DLHJ) have demonstrated significant advantages over their homojunction counterparts. The use of heterostructures is also prevalent in III-V semiconductor based infrared detectors. Much has been discussed in the literature about the nBn and related devices, including XBn barrier photodetector [2, 9 , 10 , 11], "bariode" [12], and unipolar barrier photodiode [13], since the publication of the paper entitled "nBn detector, an infrared detector with reduced dark current and higher operating temperature" by Maimon and Wicks in 2006 [1]. Common to this family of devices is the unipolar barrier. The term "unipolar barrier" was coined recently to describe a barrier that can block one carrier type (electron or hole) but allows the un-impeded flow of the other [14,15,16], as illustrated in Figure 1. The concept of the unipolar barrier has been around long before they are called as such. The double-heterostructure (DH) laser, which makes use of a pair of complementary unipolar barriers, was first described in 1963 [17,18], soon after the birth of the concept of heterostructure devices. Unipolar barriers have also been used to enhance infrared detector performance. A unipolar barrier can be used to impede the flow of majority carrier dark current in photoconductors [19]. A DH detector design, depicted in Figure 1, can be used to reduce diffusion dark current emanating from the diffusion wings surrounding the absorber layer [20]. The nBn [1,21,22] (see Figure 1) or XBn [2,9,10,23] detector structure uses a unipolar barrier to suppress dark current associated with Shockley-Read-Hall processes without impeding photocurrent flow, as well as to suppress surface leakage current [22]. In general, unipolar barriers can be used to implement the barrier infrared detector architecture for increasing the collection efficiency of photo-generated carriers, and reducing dark current generation without inhibiting photocurrent flow. The nBn detector serves as good example for illustrating the use of unipolar barriers.

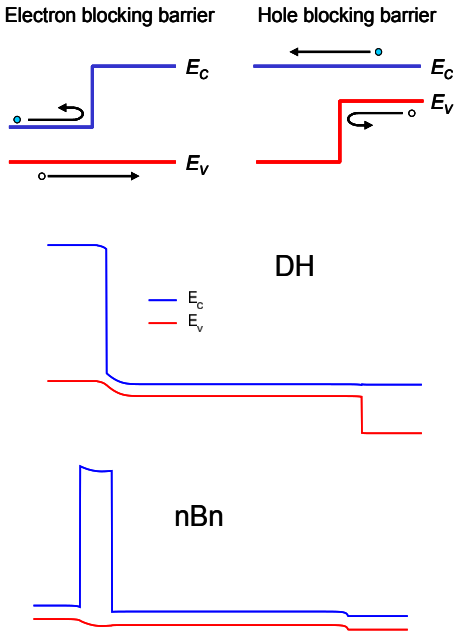

Figure 1. Schematic illustrations of electron- and hole-blocking unipolar barriers, and two examples of unipolar barrier based device structures: double heterostructure (DH), and nBn

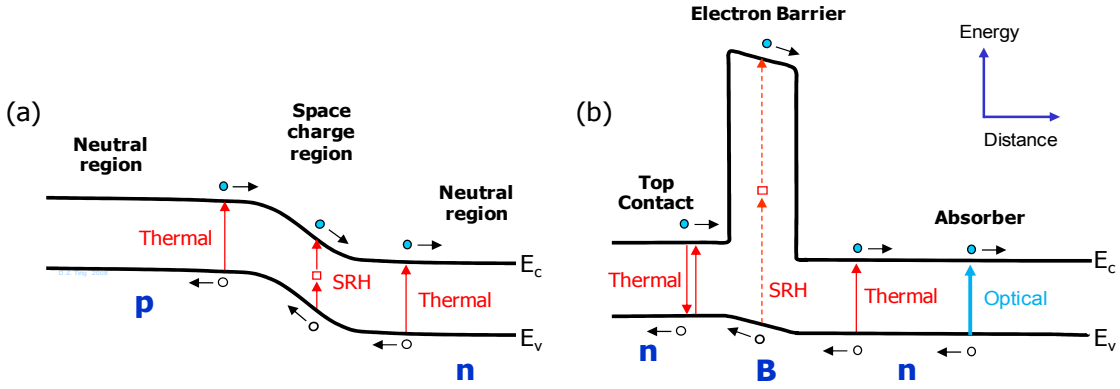

Figure 2. Schematic energy band diagram showing the conduction and valence band edges (E_c and E_v) of (a) a p-n junction photodiode, and (b) an nBn barrier infrared detector.

The nBn barrier infrared detector concept was first described by Shimon Maimon and Gary W. Wicks at the 11th International Conference on Narrow Gap Semiconductors in 2003 [21]. The basic operating principles of the nBn and the related XBn detectors have been described in detail in the literature [2,9,10,11,22]. Here we summarize some key points. The nBn infrared detector is designed to reducing dark current (noise) without impeding photocurrent (signal). The energy band diagram of a typical nBn barrier infrared detector structure is shown in Figure 2(b). It has an n-doped top contact, a unipolar electron Barrier, and a lightly n-doped infrared (IR) absorber region (hence the name "nBn"). It somewhat resembles the typical p-n photodiode shown in Figure 2(a), except that the junction (space charge region) is replaced by an electron blocking unipolar barrier (B), and that the p-contact is replaced by an n-contact. Figure 2 (b) also shows that photo-generated electrons and holes in the absorber of the nBn detector can flow to the left and the right, respectively; neither is blocked by the barrier.

The barrier is highly effective in dark current suppression. In particular, the barrier serves to reduce surface leakage current. In a typical pn junction array, the detectors are defined by etching past the depletion region for pixel isolation. The exposed small-band-gap semiconductor sidewalls are a source of surface leakage dark current, which often require passivation for suppression. The nBn detectors require only a shallow etch past the top contact layer to expose the wide-gap barrier, where surface leakage current is suppressed; this eliminates the need for surface passivation [1]. Even in a deep-etched mesa configuration, where the side walls of the narrow gap absorber are fully exposed, the barrier can still block electron surface leakage effectively [9,13,22,24].

The nBn detector is designed such that replacement of the p-contact in the pn junction by the n-contact/barrier combination does not lead to additional majority carrier dark current from the top contact. As illustrated in Figure 2 (b), the unipolar barrier serves to block the flow of electron (majority carrier) dark current from the top n-contact. The electrons blocked by the barrier eventually recombine with the thermally generated holes so that there is no flow of electron dark current from the top contact layer.

Central to the nBn operation is the strong suppression of generation-recombination (G-R) dark current due to Shockley-Read-Hall (SRH) processes. As discussed by Kilpstein [2], in a conventional photodiode, there exists a threshold temperature T_0, above which the dark current is diffusion limited, and below which it is G-R limited. In a homojunction pn diode, the G-R current, which is proportional to $\exp(-E_g / 2kT)$ (assuming mid-gap defect level), is predominantly generated in the depletion region. The suppression of the G-R dark current allows the detector to operate at higher temperature, or with higher sensitivity. In the nBn, where the depletion region is replaced by a larger gap semiconductor, in which the $\exp(-E_g / 2kT)$ factor is greatly reduced (particularly at lower temperatures), the SRH dark current generation is virtually eliminated. This is illustrated in Figure 3, where the SRH recombination rates at T=80K are obtained by heterojunction drift-diffusion simulation [25] for a pn diode and an nBn structure, both with $InAs_{0.91}Sb_{0.09}$, which is lattice matched to GaSb substrate, as the MWIR absorber. The doping in the p and n regions of the homojunction diode are taken to be p=1×10^{16} cm^{-3} and n=1×10^{16} cm^{-3}, respectively. The absorber doping of the nBn structure is n=1×10^{16} cm^{-3}, while a 2000 Å wide AlSbAs barrier (B) is undoped. A value of $\tau_p = \tau_n = 100$ ns is used in the simulation. The reverse bias energy band diagrams for the two devices are shown, along with the calculated magnitudes (i.e., the absolute values) of the SRH recombination rates, given by the expression: $r_{SRH} = (np - n_i^2) / [(\tau_p (n + n_i) + (\tau_n (p + p_i)]$.

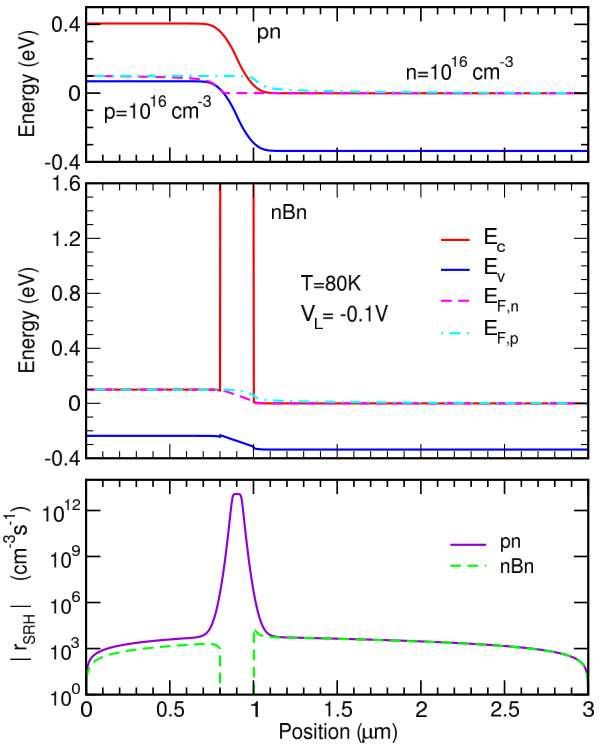

Figure 3. The top and middle panels show the calculated 80K reverse-bias energy diagrams along with quasi Fermi levels for an InAsSb based MWIR pn junction diode and an nBn detector, respectively. The bottom panel shows the calculated magnitude of the Shockley-Read-Hall recombination rates for the two structures as functions of position.

For the pn junction the calculated peak SRH generation rate in the middle of the depletion region is approximately 10 orders of magnitude larger than the baseline rate outside the depletion region. In contrast, for the nBn structure the calculated peak SRH generation rate in the barrier is essentially zero. In the nBn structure, there is virtually no SRH generation in the barrier region. A small amount of SRH generation is found in the nBn absorber region, due to the small bias drop over the absorber, but the size is negligible when compare to the SRH generation rate in the homojunction.

3. QUANTUM DOT BARRIER INFRARED DETECTOR (QD-BIRD)

The standard nBn device uses a lattice-matched InAsSb absorber grown on GaSb substrate, with cutoff wavelengths of ~4.2 μm at T=150K [1]. While this detector could operate at much higher temperatures than existing MWIR detectors based on InSb, its spectral responses do not cover the full (3 – 5 μm) MWIR atmospheric transmission window. Here we describe a simple approach to extending the cutoff wavelength of the standard nBn detector by insert quantum dots into the absorber layer of the nBn.

The layer diagram in Figure 4 shows the growth sequence of the QD-BIRD. The energy band diagram schematically illustrates the structure of the quantum dot barrier infrared detector (QD-BIRD). It is very similar to the standard nBn device structure as originally described by Maimon and Wicks [1,21], consisting of an AlSbAs barrier sandwiched between the InAsSb top contact layer and absorber layer. The slight modification we introduced is the periodic insertion of 2.8 monolayers (MLs) of InSb, which forms self-assembled InSb quantum dot layers in the InAsSb absorber matrix, as illustrated in Fig. 5. The alloy composition of the InAsSb matrix was adjusted slightly to reduce the Sb content. Details of the structure have been reported earlier [5].

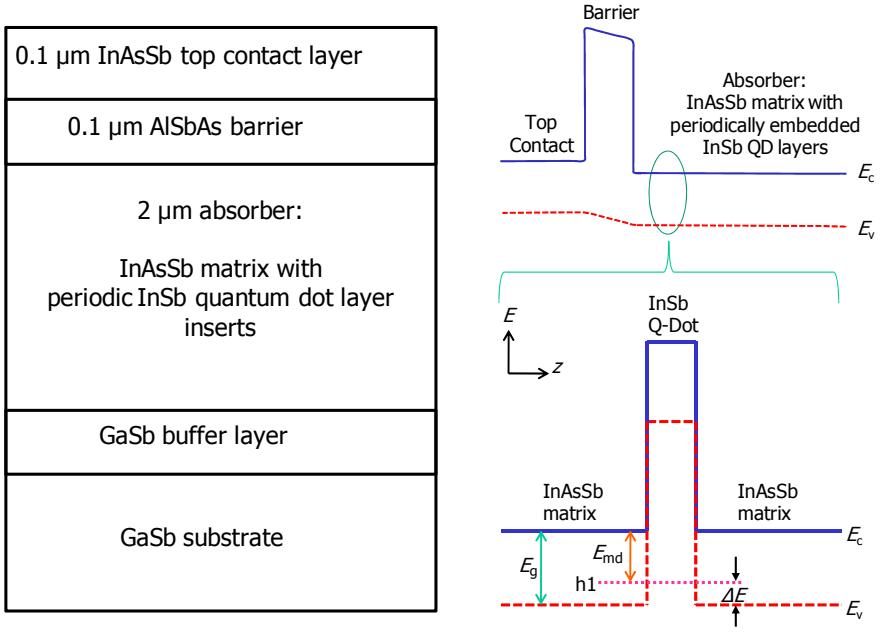

Figure 4. The left panel show the QD-BIRD device layer diagram. The top-right panel shows the schematic energy band diagram of the active region of the QD-BIRD device. The bottom-right panel shows the schematic energy band diagram for the QD-BIRD absorber near an InSb quantum dot layer.

Figure 5 shows the normalized photoluminescence (PL) spectrum of the QD-BIRD with two distinct peaks at 4.0 µm and the 5.5 µm. The origins of the two peaks are illustrated in the bottom right panel of Figure 4, which shows the schematic energy band diagram in the vicinity of an InSb quantum dot insertion layer in the InAsSb matrix. The 4.0 µm peak is easily identified with the band gap E_g of the InAsSb matrix. The 5.5 µm peak is related to the quantum dot. The band diagram shows that the strained InSb forms a type-II broken gap band alignment with the InAsSb matrix, with both the conduction and valence band edge of InSb being substantially higher than the conduction band edge of InAsSb. The InSb quantum conduction band state is clearly unconfined and therefore is not likely a source of the PL peak. What is most probably responsible for the 5.5 µm PL peak is a type-II transition involving the conduction band edge of the InAsSb matrix, and the confined hole state of the InSb quantum dot. This transition is illustrated in bottom right panel of Figure 4, and is labeled E_{md}.

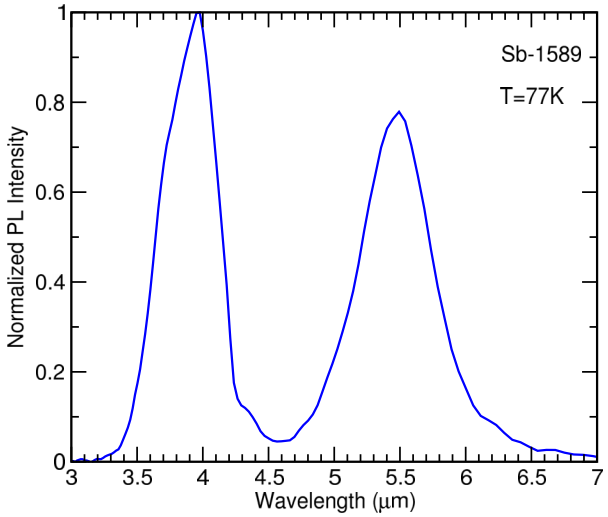

Figure 5. Photoluminescence (PL) spectrum for the QD-BIRD taken at T=77K.

Figure 6 shows the spectral quantum efficiency for a QD-BIRD device, without AR coating, taken at 125K, 175K, and 225K under -200 mV bias. The spectral response is measured using a top-illuminated geometry. Because the GaSb substrate is essentially transparent to the MWIR radiation under consideration, the spectral response should be considered as a double-pass (or multiple-pass) result, since after passing through the absorber initially, light could re-enter the absorber region after reflecting off the bottom of the substrate. Like the PL spectrum, the spectral responsivity also shows a distinct bimodal behavior. The photo-response associated with the direct band-to-band transition in the InAsSb matrix is seen at the shorter wavelengths, with approximate plateau quantum efficiency values of 0.33, 0.55, and 0.61 at T=125K, 175K, and 225K, respectively. For this InAsSb matrix responsive, the 50% quantum efficiency cutoff wavelengths are approximately 4.15, 4.30, and 4.46 µm at T=125K, 175K, and 225K, respectively.

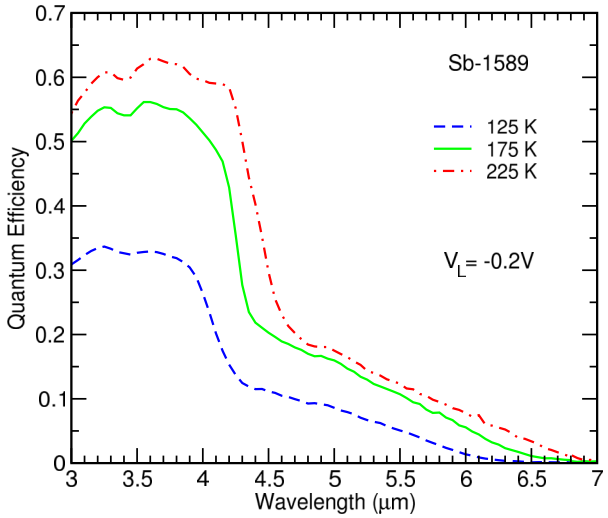

Figure 6. Multi-pass spectral quantum efficiency of a QD-BIRD without anti-reflection coating taken under -0.2 V applied bias, measured at 125K, 175K, and 225 K.

Beyond this cutoff wavelength associated with the bulk InAsSb matrix, we also observe extended response which drops off approximately linearly; this is attributed to the type-II transition between the quantum dot valence band state and the InAsSb matrix conduction band state. The extended response associated with the quantum dots is noticeably weaker than the bulk InAsSb response. The external quantum efficiencies at 5 µm for T=125K, 175K, and 225K are respectively 0.086, 0.16, and 0.175, which are only approximately 26 - 31% the corresponding values found for the InAsSb matrix in the 3-4 µm range, even though the PL intensities of the QD-to-matrix and the bulk transitions are comparable. One reason for the weaker response of the QD-to-matrix transition is that the quantum dot hole state is confined by the InAsSb matrix. The confinement energy ΔE is given by the difference between the InAsSb band gap E_g and the QD-to-matrix transition energy E_{md} (see Figure 4). The photo-excited hole (minority carrier) in the quantum dot has to overcome this additional energy barrier ΔE in order to escape and be collected. There is likely a distribution of quantum dot sizes, with a corresponding distribution E_{md} and ΔE. Smaller dots with smaller E_{md} that lead to longer the extended wavelength would need a larger activation energy ΔE. for the photo-generated hole to escape; this is associated with a lower escape probability. This would explain why the extended cutoff response decreases as the wavelength increases.

Figure 6 shows that the photo-response increases with temperature; the responsivity at 225K is approximately twice that at 125K. One possible mechanism responsible for this behavior is the presence of a small un-intended hole barrier resulting from the valence band mismatch between the absorber and the AlSbAs barrier (the valence band edges of the absorber and the barrier should be aligned in an ideal nBn structure). This barrier would block photo-currents generated from both the InAsSb matrix absorption and the dot-to-matrix absorption. Another possibility is that the quantum dots themselves could impede minority carrier transport. An unoccupied QD could also trap holes. A QD occupied by a hole is a (screened) Coulomb scattering center, which in principle could provide the observed temperature dependence.

Figure 7 shows the measured dark current density for a QD-BIRD as a function of applied bias at 125K, 175K, and 240K. The reverse-bias (negative top contact bias) current-voltage characteristics appear diffusion-limited at 175K and 240K. Under -200 mV bias, the dark current density levels are 1.52×10^{-7} A/cm^2 and 3.77×10^{-4} A/cm^2, respectively at 125K and 175K. We computed the black-body specific detectivity (D^*) for f/2 optics, 300 K background conditions. The photocurrent is determined from the integrated photo-response in the 3 μm to 6 μm spectral range. For detector temperature of T=175K, under -200 mV bias, the black-body D^* is dark-current limited and has a value of 1.07×10^{11} cm-Hz$^{1/2}$/W. At T=125K, the black-body D^* becomes background limited and has a value of 3.76×10^{12} cm-Hz$^{1/2}$/W.

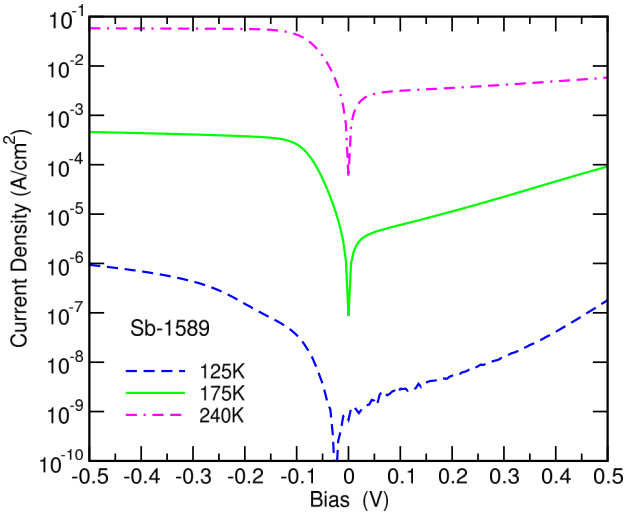

Figure 7. Dark current density as a function of applied bias of a QD-BIRD taken at 125K, 175K, and 240 K.

4. CONCLUSIONS

The nBn or XBn barrier infrared detector has the advantage of reduced dark current resulting from suppressed Shockley-Read-Hall (SRH) recombination and surface leakage. High performance detectors and focal plane arrays (FPAs) based on InAsSb absorber lattice matched to GaSb substrate, with a matching AlAsSb unipolar electron barrier, have been demonstrated. The band gap of lattice-matched InAsSb yields a detector cutoff wavelength of approximately 4.2 • μm when operating at ~150K. We report results on the quantum dot barrier infrared detector (QD-BIRD), which is a simple modification of the standard MWIR nBn detector with an InAsSb absorber lattice-matched to the GaSb substrate. We showed that by incorporating self-assembled InSb quantum dots into the InAsSb absorber matrix, we could extend the detector cutoff wavelength from ~4.2 μm to 6 μm, and thus providing better spectral coverage of the MWIR transmission window. The QD-BIRD has been observed to show infrared response at 225 K.

Acknowledgment

The authors thank M. Herman, E. Kolawa, S. Khanna, T. Cwik, and P. Dimotakis of JPL, and R. Stephan of the Game Changing Technology Division at the NASA Office of the Chief Technologist for encouragement and support. The research described in this publication was carried out at the Jet Propulsion Laboratory, California Institute of Technology, under a contract with the National Aeronautics and Space Administration.

REFERENCES

1. S. Maimon and G. W. Wicks, "nBn detector, an infrared detector with reduced dark current and higher operating temperature," *Appl. Phys. Lett*. **89**(15) 151109 (2006).

2. P. Klipstein, "'XBn' barrier photodetectors for high sensitivity and high operating temperature infrared sensors," *Proc. of SPIE*. 6940 (2008) 69402U.

3. H. S. Kim, E. Plis, J. B. Rodriguez, G. D. Bishop, Y. D. Sharma, L. R. Dawson, S. Krishna, J. Bundas, R. Cook, D. Burrows, R. Dennis, K. Patnaude, A. Reisinger, and M. Sundaram, "Mid-IR focal plane array based on type-II InAs/GaSb strain layer superlattice detector with nBn design," *Appl. Phys. Lett*. **92**(18), 183502 (2008).

4. G. Bishop, E. Plis, J. B. Rodriguez, Y. D. Sharma, H. S. Kim,L. R. Dawson, and S. Krishna, "nBn detectors based on InAs/GaSb type-II strain layer superlattice", J. Vac. Sci. Technol. B 26(3) 1145 (2008).

5. C. J. Hill, A. Soibel, S. A. Keo, J. M. Mumolo, D. Z. Ting, and S. D. Gunapala, "Mid-infrared quantum dot barrier photodetectors with extended cutoff wavelengths", *Electronics Letters* **46**(18) 1286-1288 (2010).

6. J. M. Arias, J. G. Pasko, M. Zandian, S. H. Shin, G. M. Williams, L. O. Bubulac, R. E. De Wames, and W. E. Tennant, "Planar p-on-n HgCdTe heterostructure photovoltaic detectors, " *Appl. Phys. Lett*. **62**, 976 (1991).

7. G. N. Pultz, P. W. Norton, E. E. Kruger, and M. Reine, "Growth and characterization of P-on-n HgCdTe liquid-phase epitaxy heterojunction material for 11–18 μm applications," *J. Vac. Sci. Technol. B* **9**, 1724 (1991).

8. T. Tung, L. V. DeArmond, R. F. Herald, P. E. Herning, M. H. Kalisher, D.A. Olson, R. F. Risser, A. P. Stevens, and S. J. Tighe, "State of the art of Hg-melt LPE HgCdTe at Santa Barbara Research Center," Proc. SPIE 1735,109 (1992).

9. Olga Klin, Steve Grossman, Noam Snapi, Maya Brumer, Inna Lukomsky, Michael Yassen, Boris Yofis, Alex Glozman, Ami Zemel, Tal Fishman, Eyal Berkowitz, Osnat Magen, Joelle Oiknine-Schlesinger, Itay Shtrichman, Eliezer Weiss and P C Klipstein, "Progress with Antimonide Based Detectors at SCD" Proc. Infrared Technology and Applications XXXV, SPIE 7298, 7298-0G (2009).

10. Philip Klipstein, Olga Klin, Steve Grossman, Noam Snapi, Barak Yaakobovitz, Maya Brumer, Inna Lukomsky, Daniel Aronov, Michael Yassen, Boris Yofis, Alex Glozman, Tal Fishman, Eyal Berkowicz, Osnat Magen, Itay Shtrichman, and Eliezer Weiss, " 'XBn' Barrier Detectors for High Operating Temperatures", Proc. of SPIE Vol. 7608, 76081V (2010).

11. Philip Klipstein, Olga Klin, Steve Grossman, Noam Snapi, Inna Lukomsky, Daniel Aronov, Michael Yassen, Alex Glozman, Tal Fishman, Eyal Berkowicz ,Osnat Magen, Itay Shtrichman, and Eliezer Weiss, "XBn barrier photodetectors based on InAsSb with high operating temperatures", Optical Engineering 50(6), 061002 (2011)

12. Philip Klipstein, Olga Klin, Steve Grossman, Noam Snapi, Inna Lukomsky, Maya Brumer, Michael Yassen, Daniel Aronov, Eyal Berkowitz, Alexander Glozman, Tal Fishman, Osnat Magen, Itay Shtrichman, and Eliezer Weiss, "MWIR InAsSb XBn detector (bariode) arrays operating at 150K", Proc. SPIE 8012, 80122R (2011)

13. G. R. Savich, J. R. Pedrazzani, D. E. Sidor, S. Maimon, and G. W. Wicks, "Dark current filtering in unipolar barrier infrared detectors", Appl. Phys. Lett. 99, 121112 (2011).

14. D. Z.-Y. Ting, S. V. Bandara, J. Mumolo, S. A. Keo, J. Nguyen, H.C. Liu, C.Y. Song, Y.-C. Chang, S. B. Rafol, C. J. Hill, S. D. Gunapala, A. Soibel, J. K. Liu, E. Blazejewski, "Dots, QWISPs, and BIRDs," *Infrared Physics & Technology*, **52**(6), 294-298 (2009).

15. David Z.-Y. Ting, Sumith V. Bandara, Cory J. Hill, Sarath D. Gunapala, Yia-Chung Chang, H. C. Liu, C. Y. Song, Alexander Soibel, Jason Mumolo, Jean Nguyen, John K. Liu, Sam A. Keo, Sir B. Rafol, and E. R. Blazejewski, "Novel quantum well, quantum dot, and superlattice heterostructure based infrared detectors", *Infrared Technology and Applications XXXV*, edited by Bjørn F. Andresen, Gabor F. Fulop, Paul R. Norton, *Proc. of SPIE* Vol. **7298**, 729805, (2009).

16. D. Z.-Y. Ting, C. J. Hill, A. Soibel, S. A. Keo, J. M. Mumolo, J. Nguyen, and S. D. Gunapala, "A high-performance long wavelength superlattice complementary barrier infrared detector," *Appl. Phys. Lett.* **95**, 023508 (2009).

17. H. Kroemer, "A proposed class of heterojunction injection lasers," *Proc. IEEE* **51**(12), 1782 (1963).

18. Zh. I. Alferov, R. F. Kazarinov, Inventor's Certificate No. 181737 (in Russian), Application No. 950 840 (1963).

19. A. M. White, "Infra red detectors," U. S. Patent No. 4,679,063 (7 July 1987).

20. M. Carras, J. L. Reverchon, G. Marre, C. Renard, B. Vinter, X. Marcadet, and V. Berger, "Interface band gap engineering in InAsSb photodiodes," *Appl. Phys. Lett.* **87**(10) 102103 (2005)

21. S. Maimon and G. W. Wicks, "InAsSb/GaAlSb/InAsSb nBn IR detector for the 3-5μm", 11th International Conference on Narrow Gap Semiconductors, June 16-20, 2003, Buffalo, New York (abstract only).

22. J. R. Pedrazzani, S. Maimon and G. W. Wicks, "Use of nBn structures to suppress surface leakage currents in unpassivated InAs infrared photodetectors," *Electronics Lett.* **44**(25) 1487-1488 (2008).

23. P.C. Klipstein, "Depletion-less Photodiode with Suppressed Dark Current and Method for Producing the Same" Int. Patent Publication no: WO 2005/004243 A1 (13 January 2005, priority date: 2 July 2003)

24. G. W. Wicks, G. R. Savich, J. R. Pedrazzini, S. Maimon, "Infrared detector epitaxial designs for suppression of surface leakage current", Proc. of SPIE Vol. 7608, 760822 (2010).

25. E. S. Daniel, X. Cartoixà, W. R. Frensley, D. Z.-Y. Ting, and T. C. McGill, "Coupled Drift-Diffusion/Quantum Transmitting Boundary Method Simulations of Thin Oxide Deives with Specific Application to a Silicon Based Tunnel Switch Diode," *IEEE Trans. Electron Devices* **47**(5), 1052-1060 (2000).